

Frequency dependent directivity of guided waves excited by circular transducers in anisotropic composite plates

Evgeny Glushkov, Natalia Glushkova, and Artem Eremin^{a)}

*Institute for Mathematics, Mechanics and Informatics, Kuban State University,
Krasnodar 350040, Russia*

evg@math.kubsu.ru, nvg@math.kubsu.ru, eremin_a_87@mail.ru

Rolf Lammering and Mirko Neumann

*Institute of Mechanics, Helmut-Schmidt-University/University of the Federal Armed Forces,
Hamburg, D-22043 Hamburg, Germany*

rolf.lammering@hsu-hh.de, mirko.neumann@hsu-hh.de

Abstract: Lamb wave propagation in fiber-reinforced composite plates is featured by a pronounced directivity of wave energy transfer along the fibers from a point surface source. In the case of non-point (sized) source, the main lobe of radiation diagram may turn with frequency up to the orthogonal to the fibers direction. This effect has been theoretically studied and physically explained in the context of semi-analytical integral-equation based mathematical model. The present paper gives its experimental verification.

© 2012 Acoustical Society of America

PACS numbers: 43.35.Zc, 43.20.Rz, 43.20.Mv [JM]

Date Received: March 5, 2012 **Date Accepted:** June 20, 2012

1. Introduction

Ultrasonic structural health monitoring (SHM) of plate-like engineering structures is based on the guided wave (GW) ability to propagate over plates for long distances inspecting their real state in a nonintrusive manner.¹⁻⁴ Whereas for isotropic structures the inspection methodology has been theoretically well grounded, anisotropic nature of modern layered polymer-based composite materials (e.g., carbon fiber-reinforced laminates) results in more challenging problems for predictive simulation. In contrast to isotropic materials, the patterns of GWs generated in anisotropic structures are featured by additional spatial angular dependencies of dispersion and amplitude characteristics. In particular, even with an axially symmetric source, a focusing of wave energy transfer in certain directions of GW propagation from the source may occur.

Experimental and theoretical study of these phenomena, carried out for laminate plates with different lay-ups driven by a focused ultrasonic beam, has revealed that the maximum GW amplitude is formed along the fiber orientation in the upper (forced) unidirectional sublayer.⁵ Similar qualitative results were obtained based on the far field approximation of three-dimensional Green's function derived for cross-ply laminates excited by a point source.^{6,7} It is worthy to note that the radiation patterns obtained for point sources are weakly frequency dependent and so they exhibit such preferable directivity along the upper fibers in the whole frequency range considered.

On the other hand, with a dimensional source, the radiation pattern becomes more complex and frequency dependent. In particular, semi-analytical integral-equation based modeling of GW generation by a circular piezoelectric wafer active sensor (PWAS) in a cross-ply laminate has revealed a possibility of maximum wave energy outflow in the direction orthogonal to the upper-ply orientation.⁸ The change of the

^{a)} Author to whom correspondence should be addressed.

transducer radius at a fixed excitation frequency also results in a variation of GW directivity.⁹ Detailed theoretical study¹⁰ has shown that with a frequency increase, the main radiation lobe periodically alternates either along the upper-ply fibers or in the perpendicular direction. The period of alternation is inversely proportional to the source diameter $2a$. The latter suggested that, the same way as in the isotropic case,¹¹ the optimal for GW amplitude maximization frequencies (“sweet spots”⁴ occurred at the specific diameter-to-wavelength ratios $2a/\lambda$ yielding the in-phase superposition of the GWs generated by the two opposite actuator’s edges. In anisotropic plates, the wavelength λ depends on the direction of GW propagation, hence the optimal frequencies also vary depending on the direction.

The present short paper is intended to give an experimental confirmation of this effect. It has been implemented following the predictions obtained within the semi-analytical mathematical model of GW generation and propagation in anisotropic laminate plates.^{8,10} Section 2 gives a brief description of this model. Its more detailed description and discussion of theoretically obtained effects can be found in Refs. 8 and 10. Section 3 provides specific details of the experimental procedure, while a comparative discussion of the theoretical and experimental results, confirming the effect of GW frequency dependent directivity, is given in Sec. 4.

2. Mathematical model

The theoretical modeling has been performed in the context of general linear elasticity for three-dimensional anisotropic solids. It is assumed that the laminate structure occupies the domain $D = \cup_{m=1}^M D_m : |x| < \infty, |y| < \infty, -H \leq z \leq 0$ in the Cartesian coordinates $\mathbf{x} = (x, y, z) \equiv (x_1, x_2, x_3)$. The composite is fabricated from elastic anisotropic homogeneous plies occupying the sublayers $D_m: z_{m+1} \leq z \leq z_m$. The sublayers are perfectly bonded with each other; the outer sides $z=0$ and $z=-H$ are stress-free, except within a circular contact area Ω to which a PWAS is attached (Fig. 1). Under a driving electric field, the PWAS produces radial deformation that causes a radial surface shear tension $\tau_r(x, y)$ in the contact area. In the range of SHM working frequencies (up to 500–700 kHz), the PWAS action may be appropriately simulated by a surface load \mathbf{q} taken in the form of δ -like distribution along the PWAS edges.⁴ Therefore, with the circular PWAS under consideration, the contact stresses have been approximated by the surface radial tension (RT)

$$\mathbf{q} = \{\tau_r \cos \varphi, \tau_r \sin \varphi, 0\}, \quad \tau_r = \delta_r(r - a), \quad (1)$$

where δ_r is the ring delta-function possessing the property

$$2\pi \int_0^\infty f(r) \delta_r(r - a) r dr = f(a), \quad r = \sqrt{x^2 + y^2}.$$

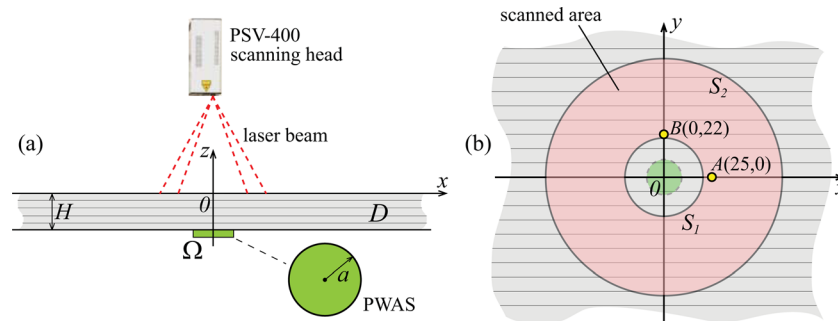


Fig. 1. (Color online) Sketch of the experimental setup: (a) side view and (b) top view.

Transient displacements $\mathbf{u}(\mathbf{x}, t)$ generated by a given surface load \mathbf{q} are expressed through the time-harmonic spectrum $\mathbf{u}(\mathbf{x}, \omega)e^{-i\omega t}$ in terms of the inverse Fourier transform over the angular frequency ω . The time-harmonic response $\mathbf{u}(\mathbf{x}, \omega) = (u_x, u_y, u_z) \equiv (u_1, u_2, u_3)$ obeys the elastodynamic equations

$$C_{ijkl}u_{i,jk} + \rho\omega^2 u_i = 0, \quad i=1, 2, 3, \tag{2}$$

holding in the sublayers D_m with specific values of material constants. Thereby, the elastic stiffness tensor components C_{ijkl} and density ρ are piecewise constant functions of the transverse coordinate z . The angular frequency $\omega = 2\pi f$, where f is frequency in kilohertz; the time-harmonic factor $e^{-i\omega t}$ is conventionally omitted.

The geometry of the problem allows one to apply the integral Fourier transform \mathcal{F}_{xy} over the horizontal spatial variables x, y and to obtain the explicit solution in terms of the inverse Fourier two-fold path integral. With the polar coordinates (r, φ) and (α, γ) : $x = r \cos \varphi$, $y = r \sin \varphi$ and $\alpha_1 = \alpha \cos \gamma$, $\alpha_2 = \alpha \sin \gamma$, it takes the form

$$\mathbf{u}(\mathbf{x}) = \frac{1}{(2\pi)^2} \int_{\Gamma_+} \int_0^{2\pi} K(\alpha, \gamma, z) \mathbf{Q}(\alpha, \gamma) e^{-i\alpha r \cos(\gamma - \varphi)} d\gamma \alpha d\alpha, \tag{3}$$

where $K = \mathcal{F}_{xy}[k]$ and $\mathbf{Q} = \mathcal{F}_{xy}[\mathbf{q}]$ are Fourier symbols of the Green matrix $k(\mathbf{x})$ and of the contact stress vector $\mathbf{q}(x, y)$. For the RT source (1), $\mathbf{Q}(\alpha, \gamma) = iJ_1(\alpha l) \{\cos \gamma, \sin \gamma, 0\}$, where J_1 is the Bessel function. The integration path Γ_+ goes in the complex plane α along the real semiaxis $\text{Re } \alpha \geq 0$, $\text{Im } \alpha = 0$, bypassing real poles $\zeta_n = \zeta_n(\gamma) > 0$ of the matrix K elements according to the principle of limiting absorption. Using the residue technique and the stationary phase method, integral representation (3) is brought to the asymptotic expansion in terms of guided waves \mathbf{u}_n

$$\mathbf{u}(\mathbf{x}) = \sum_{n=1}^{N_r} \mathbf{u}_n(\mathbf{x}) + O((\zeta_n r)^{-1}), \quad \zeta_n r \rightarrow \infty, \quad \mathbf{u}_n(\mathbf{x}) = \sum_m \mathbf{a}_{nm}(\varphi, z) e^{is_{nm}r} / \sqrt{\zeta_n r}. \tag{4}$$

The amplitude factors \mathbf{a}_{nm} are expressed via the residues of the product $K\mathbf{Q}$ from the real poles ζ_n ; $s_{nm} = s_n(\gamma_m)$ are wavenumbers of the GWs \mathbf{u}_n ; γ_m are the stationary points of the phase functions $s_n(\gamma) = \zeta_n(\gamma + \varphi + \pi/2) \sin \gamma$: $s'_n(\gamma_m) = 0$; N_r is the number of real poles ζ_n .

The shapes of the GW amplitude dependencies on the depth z , provided by the vector-functions $\mathbf{a}_{nm}(\varphi, z)$, coincide with the modal eigenforms derived using the modal analysis technique.¹² Whereas the eigenforms are obtained to a constant factor accuracy, the amplitudes \mathbf{a}_{nm} are uniquely determined for a given source \mathbf{q} which characteristics are strictly taken into account via the \mathbf{Q} factors.

3. Experimental procedure

A unidirectional plate with the lay-up $[0^\circ]_4$ and the dimensions $1000 \times 1000 \times 2.25 \text{ mm}^3$ has been used in the experiments. It was manufactured by Carbotec GmbH (Essen, Germany) from transversally isotropic prepregs with the following mechanical properties:

$$C_{11} = 109.3, \quad C_{22} = 13.8, \quad C_{12} = C_{13} = 7.0, \quad C_{23} = 5.8, \quad C_{55} = C_{66} = 4.4 \text{ (GPa)}, \\ \rho = 1500 \text{ (kg/m}^3\text{)}.$$

(The elastic constants are given here in conventional two-index Voigt notation.) The plate is driven by a circular vertically polarized piezoceramic actuator (PIC151 ceramic, PI Ceramic GmbH, Lederhose, Germany) placed at its center (radius of the electrode area $a = 7.8 \text{ mm}$, thickness $b = 0.25 \text{ mm}$). The actuator is adhered to the plate's surface

with super glue (Loctite 401, Henkel AG & Co. KGaA, Düsseldorf, Germany) and the laminate is placed on a rigid lightweight foam to provide stress-free boundary conditions as in the mathematical model used.

The velocity field of propagating waves is captured on the opposite side of the plate by means of a Polytec PSV-400 scanning laser vibrometer (Polytec GmbH, Waldbronn, Germany) coupled with a TDS 1012B two-channel digital storage oscilloscope (Tektronix Inc., Beaverton, OR). The scanning head of the PSV-400 system is placed 1.312 m above the specimen. A thin reflective film is glued to the surface of the plate in the area of observation, which is proved to be a suitable tool for improving the laser beam reflection and minimizing the signal-to-noise ratio.

The actuator is excited by a five-cycle Hann windowed sine tone-burst with a repetition rate varying from 30 ms for low frequencies to 2 ms for higher ones. For this purpose a Tektronix AFG 3022B two-channel arbitrary signal generator is used. The generated signal is amplified (HSA-4014 amplifier, NF Corporation, Yokohama, Japan) to the amplitude $100V_{pp}$ before it is applied to the actuator. To observe the influence of source size and material anisotropy on GW propagation patterns, circular-shape areas adjacent to the actuator are scanned by the vibrometer and root mean square (RMS) values for the detected signals are calculated. At every measurement point the signal is averaged 50 times. To obtain frequency response in various propagation directions, the actuator is driven by a periodic chirp generated by the vibrometer hardware and covering the range from 10 kHz to 250 kHz. The fast Fourier transform is then applied to the measured signals.

4. Results and discussion

To reveal the source influence on the GW directivity, two points $A(25,0,0)$ and $B(0,22,0)$ (mm) in the directions along and across the fibers has been selected on the plate's surface for the frequency response measurement and simulation [Fig. 1(b)]. The solid and dashed lines in Fig. 2(a) depict the out-of-plane velocity magnitude $|v_z| = \omega|u_z|$ versus the frequency f measured at the points A and B , respectively. To demonstrate the influence of the actuator's size, the lower subplot of Fig. 2 shows the structure's response on the vertical point load $\mathbf{q} = \{0, 0, \delta(x, y)\}$ calculated at the same points A and B .

The top curves exhibit typical alternations of maxima and minima, similar to those presented in Fig. 12 from Ref. 10 for circle sources of different size. On the contrary, the point load yields smooth dependencies with a higher response in the fiber

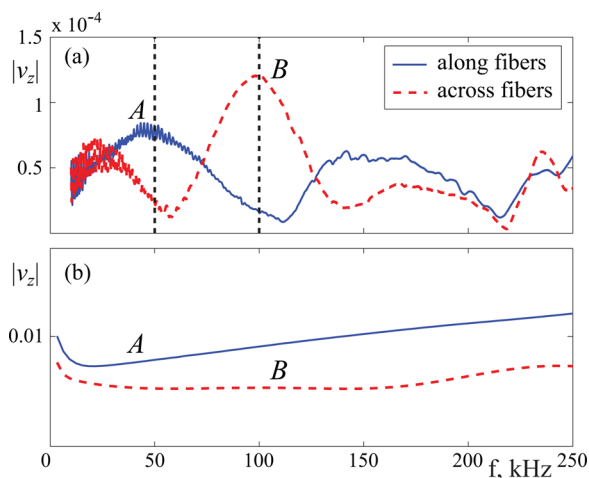


Fig. 2. (Color online) Frequency spectrum of the out-of-plane velocity amplitudes $|v_z|$ at the points A (direction along fibers, solid lines) and B (across fibers, dashed lines); (a) PWAS of radius $a = 7.8$ mm (experimental measurements), (b) vertical point load (theoretical calculations).

Table 1. Experimental (f_{\min}, f_{\max}) and predicted ($\hat{f}_{\min}, \hat{f}_{\max}$) frequencies (in kHz) of minimal and maximal out-of-plane velocity amplitudes $|v_z|$ for GWs propagating along (A) and across (B) fibers.

	f_{\min}	\hat{f}_{\min}	f_{\max}	\hat{f}_{\max}
A :	110.5	99.5	43.3	42.8
	215.3	212.7	147.5	160.2
B :	57.5	50.9	22.6	19.2
	140.5	128.0	98.3	88.7
	218.4	227.5	167.5	168.8

direction in the entire frequency range. Due to the difference in wavelengths along and across fibers, local minima and maxima of the curves do not generally occur simultaneously. Moreover, the maximum in one of the directions may occur at the minimum of the counterpart curve. For example, the out-of-plane velocity amplitude measured at the point A is almost minimal at $f=100$ kHz when the response at the point B , in the orthogonal to fibers direction, reaches the top level. All the frequency points of local minima and maxima obtained experimentally (f_{\min}, f_{\max}) and theoretically ($\hat{f}_{\min}, \hat{f}_{\max}$) for the both points A and B are listed in Table 1. One can see good agreement of the predicted and measured frequencies even with so simple source model (1) not accounting for the contact stress angular variation caused by the anisotropy.

The GW directivity becomes even more visible in Fig. 3 displaying surface scans recorded using the laser vibrometer (left diagrams) and simulated using semi-analytical expressions (4) (right diagrams). It depicts the RMS values

$$v_{z,\text{RMS}}(x) = \frac{1}{M} \sqrt{\sum_{i=1}^M v_z^2(x, t_i)}$$

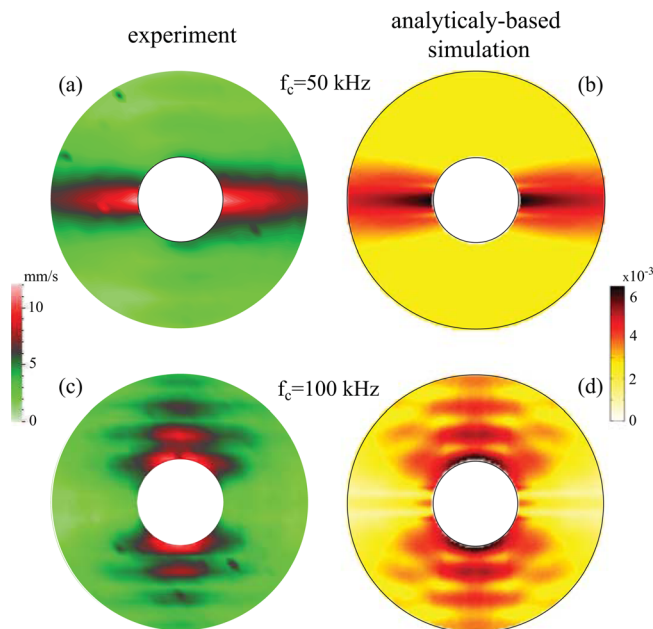


Fig. 3. (Color online) RMS for experimental (left) and computed (right) scans of the out-of-plane velocity component $v_z(x, y, 0, t)$ in the surface area around the circular PWAS [see Fig. 1(b)] illustrating the alternation of GW radiation along and across fibers (top and bottom diagrams, respectively).

for the out-of-plane velocity in the scanned area located between the circles S_1 : $r = 20$ mm and S_2 : $r = 60$ mm [see Fig. 1(b)]. The central excitation frequency $f_c = 50$ kHz of the upper subplots locates between the points $f_{\max,A}$ and $f_{\min,B}$ [see the left dashed vertical line in Fig. 2(a)]. Correspondingly, the GWs generated at this central frequency are strongly focused along the fiber direction ($\varphi = 0^\circ$ and 180°). On the contrary, for $f_c = 100$ kHz taken close to the frequencies $f_{\max,B}$ and $f_{\min,A}$ [right vertical dashed line in Fig. 2(a)], the GW amplitude concentrates in the directions $\varphi = 90^\circ$ and $\varphi = 270^\circ$, perpendicularly to the fiber orientation. A good coincidence between the experimental data and the analytically based simulation is observed here as well.

5. Conclusion

The theoretical and experimental results confirm strong frequency dependence of the GW directivity in anisotropic layered composites actuated by a sized source. It should be accounted for a proper frequency tuning of Lamb wave based SHM, PWAS grid design, etc. Noteworthy, that unlike the cross-ply samples studied earlier,^{8,10} the present results are obtained for a unidirectional specimen. It means that the presence of inner sublayers with cross-oriented fibers is not so important for a possible GW focusing in the perpendicular to the upper-ply fiber direction.

Acknowledgments

The work is partly supported by the Russian Ministry for Education and Science (project No. 10.61.2011), Deutsche Forschungsgemeinschaft, Deutscher Akademischer Austauschdienst and by the Russian Foundation for Basic Research (project No. 11-01-96508). The authors are thankful to T. Fedorkova and S. Föll (Helmut-Schmidt-University, Hamburg) for their help in the laser vibrometry experiments.

References and links

- ¹J. L. Rose, "A baseline and vision of ultrasonic guided wave inspection potential," *J. Pressure Vessel Technol.* **124**, 273–282 (2002).
- ²Z. Su, L. Ye, and Y. Lu, "Guided lamb waves for identification of damage in composite structures: A review," *J. Sound Vib.* **295**, 753–780 (2006).
- ³A. Raghavan and C. E. S. Cesnik, "Review of guided-wave structural health monitoring," *Shock Vib. Dig.* **39**, 91–114 (2007).
- ⁴V. Giurgiutiu, *Structural Health Monitoring with Piezoelectric Wafer Active Sensors* (Elsevier Academic, London, 2008).
- ⁵K. Balasubramaniam and C. V. Krishnamurthy, "Ultrasonic guided wave energy behavior in laminated anisotropic plates," *J. Sound Vib.* **296**, 968–978 (2006).
- ⁶A. Velichko and P. D. Wilcox, "Modeling the excitation of guided waves in generally anisotropic multilayered media," *J. Acoust. Soc. Am.* **121**, 60–69 (2007).
- ⁷B. Chapuis, N. Terrien, and D. Royer, "Excitation and focusing of lamb waves in a multilayered anisotropic plate," *J. Acoust. Soc. Am.* **127**, 198–203 (2010).
- ⁸Y. V. Glushkov, N. V. Glushkova, and A. S. Krivonos, "The excitation and propagation of elastic waves in multilayered anisotropic composites," *J. Appl. Math. Mech.* **74**, 297–305 (2010).
- ⁹K. S. Nadella, K. I. Salas, and C. E. S. Cesnik, "Characterization of guided-wave propagation in composite plates," *Proc. SPIE* **7650**, 76502H (2010).
- ¹⁰E. Glushkov, N. Glushkova, and A. Eremin, "Forced wave propagation and energy distribution in anisotropic laminate composites," *J. Acoust. Soc. Am.* **129**, 2923–2934 (2011).
- ¹¹E. Glushkov, N. Glushkova, R. Lammering, A. Eremin, and M. N. Neumann, "Lamb wave excitation and propagation in elastic plates with surface obstacles: Proper choice of central frequencies," *Smart Mater. Struct.* **20**, 015020 (2011).
- ¹²A. H. Nayfeh, "The general problem of elastic wave propagation in multilayered anisotropic media," *J. Acoust. Soc. Am.* **89**(4), 1521–1531 (1991).